Internuclear-separation-resolved asymmetric dissociation of I_2 in a two-color laser field

V. Tagliamonti, H. Chen, and G. N. Gibson
Department of Physics, University of Connecticut, Storrs, Connecticut 06269, USA
(Received 31 August 2011; published 24 October 2011)

We have designed a pump-probe experiment to excite I_2 to the B state and subsequently ionize the molecule with a two-color (800- and 400-nm) probe pulse. By varying the relative phase of the two colors we are able to probe the asymmetric dissociation of $I_2^{2+} \rightarrow I^{2+} + I$ and we observe spatial asymmetries in the ion yield of this (2,0) channel. Because the durations (35 fs) of the pump and probe pulses are much shorter than the vibrational period of the B state (700 fs) we can fully resolve the dynamics as a function of internuclear separation R. We find that the amplitude of the spatial asymmetry increases as a function of R and that the relative phase of the two colors that produces the maximum asymmetry is independent of R. Both of these observations are consistent with ionization of I_2 directly into the field-dressed potential curves of I_2^{2+}, which we model with a two-electron one-dimensional double-well potential in an external field. Interestingly, we find a spatial asymmetry for dissociation channels with a charge difference $\Delta q = 2$, [(2,0) and (3,1)], but not for $\Delta q = 1$, [(1,0), (2,1), (3,2)]. Finally, substructure in the time-of-flight data shows two distinct states leading to the (2,0) dissociation limit, one of which may indicate a breakdown of the presented model.

DOI: 10.1103/PhysRevA.84.043424 PACS number(s): 33.80.Rv, 32.80.Rm, 42.50.Hz

I. INTRODUCTION

Atoms and molecules have been studied in strong laser fields for decades with many kinds of experiments including above-threshold dissociation [1], symmetric and asymmetric dissociation [2–7], electronically excited fragments [8–11], and the dependence of ionization on internuclear separation [12–17]. Molecules also possess an extra degree of freedom in the form of nuclear motion, which gives rise to avoided potential energy crossings when a laser field is applied [18–20]. Furthermore, many of the dynamics observed in molecules have a strong dependence on the internuclear separation, perhaps most notably in the phenomena of enhanced ionization at a critical internuclear distance, R_c [15]. Homonuclear diatomics are particularly interesting as they exhibit charge-resonance (CR) states which couple strongly to electromagnetic fields and have no analog in atoms [21,24]. Understanding these phenomena is critical to providing a description of the complex dynamics of molecules in strong laser fields.

The CR states of a diatomic molecule play an important role in the ionization of the molecule by a strong laser field and have been extensively studied theoretically [12,22,26]. In a one-electron system, the CR states are the lowest lying states and along with electron localization produce a large increase in the ionization rate at a critical internuclear separation R_c. This phenomenon of charge-resonance-enhanced ionization (CREI) [12] appears to be universal in diatomic molecules and R_c is consistently found to be 2–3 times the equilibrium distance of the neutral molecule [15]. The CR states of an even-charged molecule are the excited ionic states which correlate to a dissociation limit with a charge difference of 2 between the fragments (e.g., $I_2^{2+} \rightarrow I^{2+} + I$). In this example, the ionic states are roughly 8 eV above the covalent ground state, although the $N_2^{6+} \rightarrow N^{4+} + N^{2+}$ dissociation channel has been observed [23], which lies 30 eV above the ground state. On the one hand, these ionic states have been identified as doorway states to ionization of even-charged molecules and produce a similar effect of R_c in odd-charged molecules [25]. On the other hand, the charge asymmetric dissociation channels which correlate with the ionic states are observed in all strong-field ionization experiments, so the ionic states are not simply doorway states but are themselves populated by the laser field. Given the high degree of excitation possible with near-IR laser fields, it is natural to ask how exactly are they populated. Unfortunately, typical time-of-flight (TOF) experiments studying the ionization and dissociation of molecules in strong laser fields simply do not have the energy resolution to separate the gerade and ungerade states that make up the CR pair, although it is the dynamics of these states that determines the response to the laser field. However, information about these states can be obtained by using $1\omega 2\omega$ fields which are created by coherently adding the fundamental and second harmonic of a laser field:

$$E(t) = E_\omega(t)\cos(\omega t) + E_{2\omega}(t)\cos(2\omega t + \phi), \qquad (1)$$

where ϕ is the relative phase between the pulses and E_ω and $E_{2\omega}$ are the envelopes of the fundamental and second harmonic, respectively (Fig. 1). This combined field can break the spatial symmetry of the interaction, which, in turn, can lead to a spatial asymmetry in the dissociation of the ionic states. From this, the amplitude and phase of the populations in the CR states can be determined.

Asymmetries produced by two-color fields have been studied theoretically [27] and experimentally [28–31] in primarily light molecules. The asymmetric dissociation of D_2 in a two-color field has been observed at ion energies identified with bond softening, rescattering, and above-threshold dissociation [31]. Similar ion yield asymmetries have been seen in H_2, N_2, HD, O_2, and CO_2 [28,29]. In these light molecules, the dynamical processes of interest occur on time scales which are on the order of the pulse duration (around 30–50 fs). One immediate consequence is that ionization and dissociation are happening in parallel. It is therefore difficult to resolve the dynamics and important information may be obscured.

This paper presents internuclear-separation-resolved measurements of the ionization of I_2 in a two-color laser field with 35-fs laser pulses, allowing us to decouple ionization

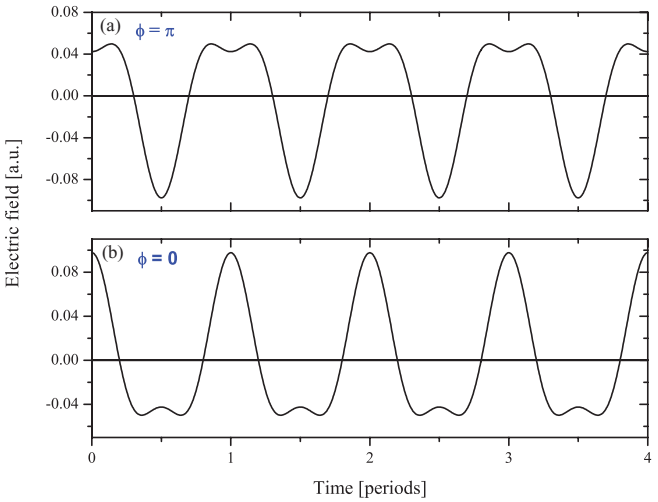

FIG. 1. (Color online) Two-color electric field $E(t) = E_\omega \cos(\omega t) + E_{2\omega}\cos(2\omega t + \phi)$ for (a) $\phi = \pi$ and (b) $\phi = 0$. The amplitudes are $E_\omega = 2E_{2\omega}$, which produces the maximum field asymmetry.

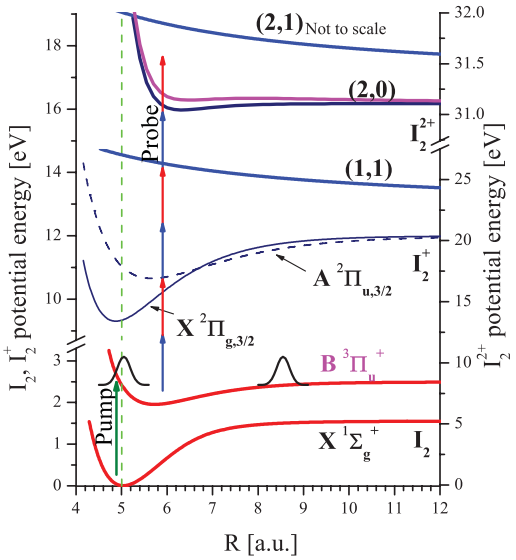

FIG. 2. (Color online) Schematic potential curves and pulse sequence. Note the two curves of the (2,0) channel corresponding to the gerade (upper) and ungerade (lower) states.

and dissociation. We do this by creating a vibrational wave packet (VWP) with a pump pulse in the B state of I_2, which evolves in time. The two-color probe pulse then ionizes the molecule at later times corresponding to different values of R. In this way, we can measure field-induced spatial asymmetries in the subsequent dissociation as a function of R. We find that the spatial asymmetry has a strong dependence on R, increasing from close to zero to almost 0.5. Moreover, the $1\omega 2\omega$ phase which produces the maximum asymmetry is independent of R. We compare these results to two models: a simple two-level model of the ionic states of a doubly charged molecule and a more complete three-level model which also includes the ground state and multiphoton excitation. We find good qualitative agreement with the two-level model, which implies direct ionization from the previous charge state to the field-dressed ionic states. However, we do find evidence of a breakdown in our quasistatic model which may be due to mechanisms such as nonadiabatic effects, electron localization, or dephasing.

Contrary to other experiments [29], we do not see any spatial asymmetry in dissociation channels where the charge difference, Δq, is one, such as the (1,0), (2,1), and (3,2) channels. In addition, we observe new features in the TOF spectrum; namely, the well-known (2,0) dissociation channel appears to consist of two distinct channels with different kinetic energy releases and different dependences of the ionization rate into the channels as a function of R.

II. EXPERIMENT

A. *R*-resolved measurements

The B state ($B^3\Pi_u^+$) of the iodine molecule is well known and is used as an intermediate state to control the internuclear separation of the molecule. The method described here and schematically represented in Fig. 2 has been studied and verified in Ref. [32]. Since the inner turning point of the B state is dependent upon the wavelength, we also have some additional control over the VWP. The wavelength of the pump pulse couples the neutral X and B states and determines the initial R position in the B state at which the vibrations begin. The vibrational period of the B state at 513 nm is around 700 fs. The pump beam resonantly excites the neutral I_2 to the B state and the $1\omega 2\omega$ probe pulse ionizes the B state at a variable time delay with a resolution of 10 fs.

The probe pulse ionizes the molecule and, depending on the intensity, can create molecular ions including I_2^+, I_2^{2+}, and I_2^{3+} [33]. Generally, the ionized molecules dissociate and the kinetic energy release of the ion fragments is measured through TOF. Identification of all measured dissociation channels of I_2 and its ions have been previously determined through correlation measurements [6]. Finally, knowing the potential curve of the B state allows us to convert from time delay to internuclear separation.

B. Experimental setup

The data collected for I_2 were obtained using a Ti:sapphire laser system. The system produces 800 μJ in 35 fs at a wavelength of 800 nm and a 1-kHz repetition rate. The beam is split by an 90:10 beam splitter to send 10% of the beam through a two-color ($1\omega 2\omega$) arm and 90% through a TOPAS (traveling-wave optical parametric amplifier of superfluorescence) system. The TOPAS is tuned to a wavelength of 513 nm and produces about 2 μJ in 50 fs. The pump and probe pulses are parallel to the TOF axis but offset in space and focused by a silver spherical mirror inside the TOF chamber to obtain spatial overlap. The pump pulse is about 1 μJ and the probe pulse has energies of 2.6 and 0.4 μJ for the 800- and 400-nm light, respectively. The intensities used are 4.3×10^{13} W/cm^2 for the 800-nm beam, 5.2×10^{13} W/cm^2 for the 400-nm beam, and 1.6×10^{13} W/cm^2 for the 513-nm beam. The 800- and 513-nm beams are both dispersion compensated with prism pairs. A computer-controlled motorized stage is used to change the time delay between the pump and probe pulses.

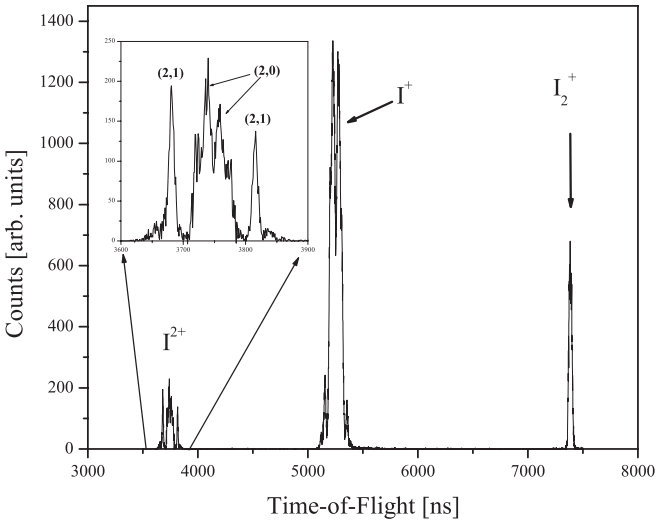

FIG. 3. TOF spectrum for a given time delay and phase showing all channels produced for the intensities used.

The iodine is introduced into the vacuum chamber effusively from a stainless-steel bulb. Experiments are done using a typical Wiley-McLaren TOF spectrometer [34]. Once the ions are produced they are extracted by a dc electric field of 223 V/cm through a 1-mm pinhole and accelerated an additional 800 eV. They are then sent through a 10-cm field-free drift tube giving both symmetric velocity dispersion and high resolution. A microchannel plate is used to detect the ions and the signal is amplified, discriminated, sent to a time-to-digital converter, and then read out to a computer. The molecules in the TOF chamber are at room temperature with a pressure of around 1×10^{-6} torr and a base pressure better than 10^{-9} torr.

The resulting TOF spectra for a particular dissociation channel consists of two peaks which are symmetric about the arrival time of the zero-kinetic-energy ion. The "forward" ("backward") peak represents ions with initial velocities toward (away from) the detector. An example of the TOF spectrum is shown in Fig. 3. The separation of the peaks is proportional to the initial momentum of the dissociating fragments.

The asymmetry of the ion yield, $\beta(\phi)$, is found by calculating the ion yield for the forward (Y_F) and backward (Y_B) peaks and is conventionally defined as

$$\beta(\phi) = \frac{Y_F(\phi) - Y_B(\phi)}{Y_F(\phi) + Y_B(\phi)}. \quad (2)$$

The asymmetry depends on ϕ and the dissociation channel. However, the difference in detection efficiency of the forward and backward ions affects $\beta(\phi)$: The backward-going ions have a larger transverse spread when they reach the extraction pinhole than the forward-going ions. As a result, the backward peaks have a smaller chance of passing through the extraction pinhole and being detected. This angular acceptance results in larger forward peaks than backward peaks since the molecules in these experiments are not perfectly aligned. However, this difference in angular acceptance was measured and accounted for.

C. Mach-Zehnder interferometer and phase measurement

The $1\omega 2\omega$ beam is produced by frequency doubling the 800-nm light with a 250-μm-thick β barium borate (BBO) crystal to generate 400-nm light. Immediately after the crystal, the 800- and 400-nm beams are separated spatially and recombined with a Mach-Zehnder interferometer designed for maximum stability (Fig. 4). Once recombined, the spatial overlap is optimized by focusing the beams and imaging them with a camera. The arm of the interferometer containing the 800-nm beam contains a $\lambda/2$ wave plate to rotate the polarization so that it is parallel with the TOF axis and the 400-nm beam. A variable attenuator in the 800-nm arm allows intensity ratios of $1\omega/2\omega$ from 1:1 up to 10:1 and controls the path difference of the two beams. Spectral interference is used to determine the relative phase of the two colors. As shown in Fig. 4, a surface reflection off of the TOF vacuum chamber window is used to send the primary 800- and 400-nm beams into a spectrometer. In order to measure the spectral interference between the two beams, the polarizations and wavelengths must be the same. To achieve this, a second BBO crystal is utilized to produce a secondary vertically polarized 400-nm beam. A polarizer projects the polarizations of the primary and secondary 400-nm beams on to the same axis and the beams can then interfere. This surface reflection allows real time measurements of the relative phase.

When the beams are properly overlapped, the interference spectrum at zero time delay shows no fringes; the overall amplitude simply goes up and down with the phase of the pulses. Thus, in order to more accurately measure the phase, fringes are produced in the spectrum by temporally offsetting the two beams with a thin piece of glass before the secondary doubling crystal. An example interference spectrum is shown in Fig. 5. The resulting spectrum is then fit with a sinusoidally modulated Gaussian and the parameter describing the relative phase is recorded for each TOF measurement. The control of the relative phase of the beams is obtained by mounting a glass variable attenuator on a motorized rotation stage which can change the phase by about 0.5 rads with each step. The interferometer has proven to be phase stable over periods of hours to better than $\pm 5^\circ$.

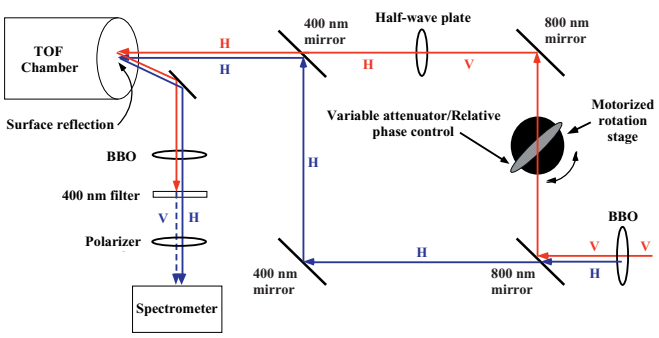

FIG. 4. (Color online) The Mach-Zehnder interferometer designed to control the relative phase of the 800- and 400-nm pulses. The polarizations of the beams are labeled as "H" and "V" for horizontal and vertical, respectively. The motorized rotation stage can change the relative phase by a minimum of 0.5 rads (about 30°).

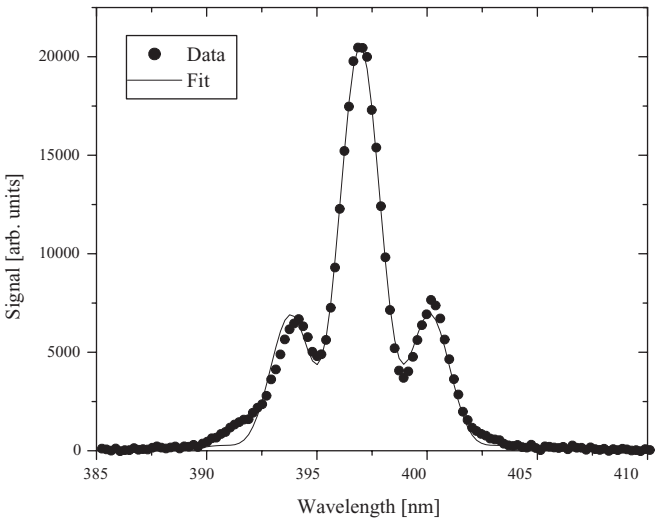

FIG. 5. Example interference spectrum used to calculate the relative phase ϕ of the $1\omega 2\omega$ field. The solid line is a sinusoidally modulated Gaussian fit.

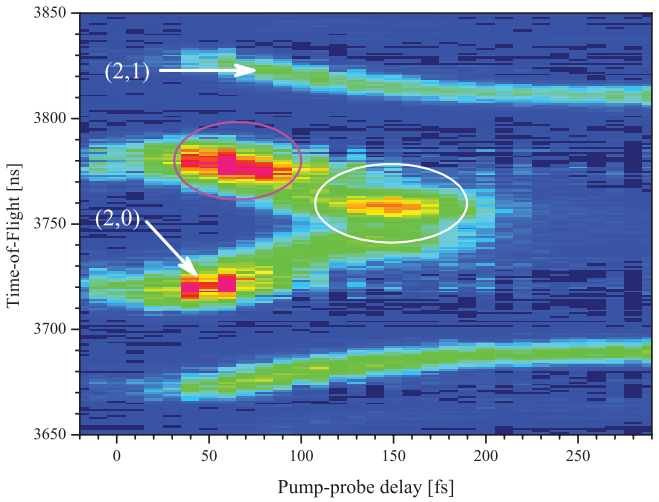

FIG. 6. (Color online) TOF as a function of the delay between the 513 nm and $1\omega 2\omega$ pulses at relative phase $\phi \approx 0$. The KER tracks for the (2,0) and (2,1) channels are labeled and the (2,0) substructures are circled. The color represents ion counts with red for higher count number and blue for lower count number.

III. EXPERIMENTAL RESULTS AND MODELS

Generally, the phase of the $1\omega 2\omega$ pulse is set and the TOF spectra are recorded for time delays of 0 to 200 fs in 10-fs steps. This is repeated for up to 18 different phase values. With this, the spatial asymmetry of any dissociation channel can be determined as a function of delay or R.

The resonant excitation to the B state is about 20% efficient, leaving roughly 80% of the population in the ground X state. Thus, the $1\omega 2\omega$ pulse can continue to ionize the X state and there are (2,0) peaks present in the TOF which are from the X state. This background is measured by blocking the 513-nm beam and subtracted from the pump-probe data, taking into account the depletion of the X state.

A typical TOF delay scan for a particular phase is presented in Fig. 6. Several features are immediately apparent. First, the image is fairly symmetric about a horizontal line at a TOF of 3748 ns corresponding to an I^{2+} ion with zero kinetic energy. The data above this line are the late (backward) ions, and below are the early (forward) ions. Second, the data form "tracks": the TOF or kinetic energy release (KER) smoothly changes with time delay, as can be seen for both the (2,0) and the (2,1) states. From Fig. 2 we see that the molecule expands in time on the B state and R increases, generally leading to lower KERs. We identify the higher KER track as the (2,1) channel, and the lower as the (2,0) channel. In fact, we verify the motion on the B state with the KER of the (2,1) channel [32]. Finally, the (2,0) channel has substructure which appears to result from two separate states. The tracks in the TOF produced from these states are shown Fig. 7(b). The clear difference in the KER observed in the TOF shows that two different (2,0) channels are being populated.

The disappearance of the (2,0) signal around 200 fs has been attributed to population trapping in the slightly bound region of the (2,0) potential curve [32,38]. The pump wavelength sets the inner turning point of the VWP and allows access to a large range of R values where trapping becomes possible. In order to discuss the experimental results in terms of R, a simulation was conducted to find the expectation value of R on the B state as a function of pump-probe delay. The results of the simulation shown in Fig. 7(a) allow conversion from pump-probe time delay to R. We find that the outer turning point on the B state is at a pump-probe delay of about 400 fs or about 8.7 a.u. as seen in Fig. 7(a). The range over which we observe the signal from I^{2+} in this experiment is from a delay of 0 to about 200 fs [solid line in Fig. 7(a)], or equivalently about 5 to 8 a.u..

The asymmetry of the (2,0) channel is found from Eq. (2). The measurement of the asymmetry for each of the (2,0) channels is found by fitting the pairs of peaks from the TOF with Gaussian curves and using the areas of the curves as the ion yield (Fig. 8). The peaks are labeled as "slow" and "fast" to distinguish the two channels. Typically, the total "left-right" asymmetry is measured [29]. Here, the left (right) is defined as the two (2,0) peaks immediately to the left (right) of the 0 KER (3748 ns). Figure 9 shows an example of the left-right asymmetry of the (2,0) channel as a function of relative phase. The asymmetry shows a clear dependence on the phase of the $1\omega 2\omega$ field with the maxima and minima separated by π, as expected. Interestingly, the (2,1), (1,0), and (3,2) do not show an asymmetry while the (3,1) channel does, in addition to the (2,0).

To examine the asymmetry dependence on internuclear separation, data sets at each R are fit to find the maximum amplitude of the asymmetry β_0 and the relative phase of the maximum ϕ_0:

$$\beta = \beta_0 \sin(\phi + \phi_0) + \beta_{\text{off}}, \tag{3}$$

where β_{off} is the offset resulting from the difference in the detection efficiency between the forward- and backward-going peaks. For left-right asymmetry, β_0 increases with R until about 7.5 a.u. when the amplitude reaches a maximum of about 0.3 (Fig. 10) and agrees qualitatively with the results of our two-level model (see the Appendix) presented in

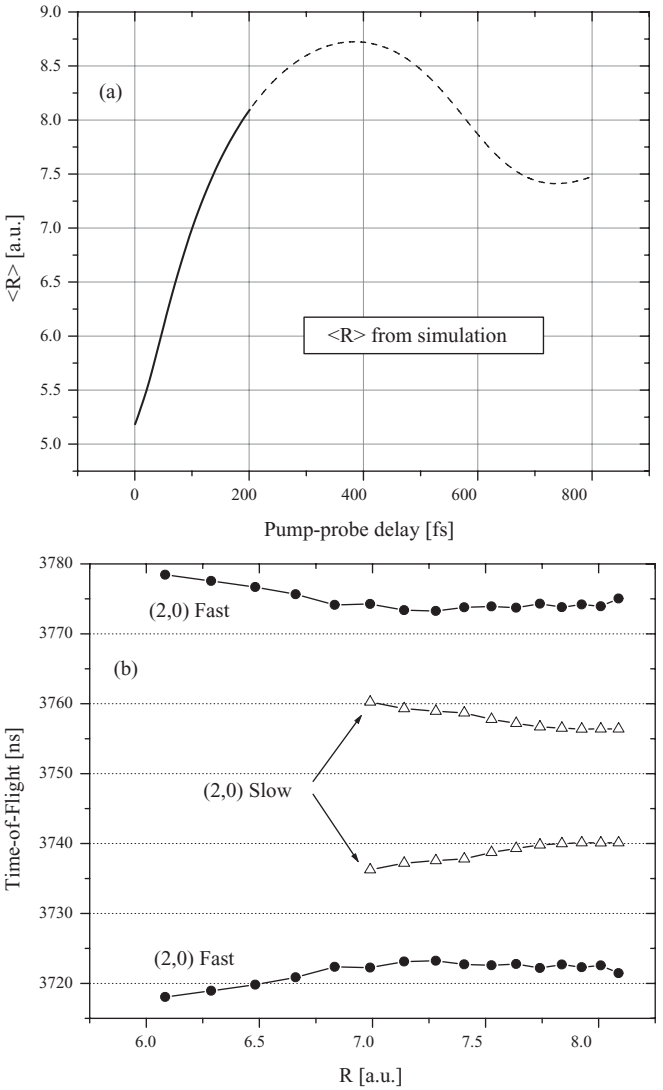

FIG. 7. (a) Simulation results for the expectation value of R vs Pump-probe delay for a VWP on the B state used to convert from time delay to R. The solid line highlights the region over which the I^{2+} signal is observed experimentally. (b) Centers of peaks for each of the (2,0) channels portraying the tracks seen in the TOF (Fig. 6) now as a function of R. The centers are found by fitting each of the peaks with a Gaussian.

Fig. 11 and discussed below. Although the amplitudes in the experimental results (Fig. 10) and the two-level calculations (Fig. 11) are different, clearly there is a region of R in which β_0 increases monotonically and a larger R region where β_0 approaches a constant maximum value. Further, the phase ϕ_0 of Eq. (3) shows no R dependence so the maximum asymmetry occurs at the same $1\omega 2\omega$ phase for each pump-probe delay (see inset of Fig. 10). This observation is in agreement with the experiments of Ref. [29] and the simple model of a two-level system presented here in which the maximum asymmetry will occur when the field itself has maximum asymmetry.

The initial measurement of the left-right asymmetry provides evidence that β_0 increases with R and ϕ_0 is constant with R as well as qualitative agreement with our two-level

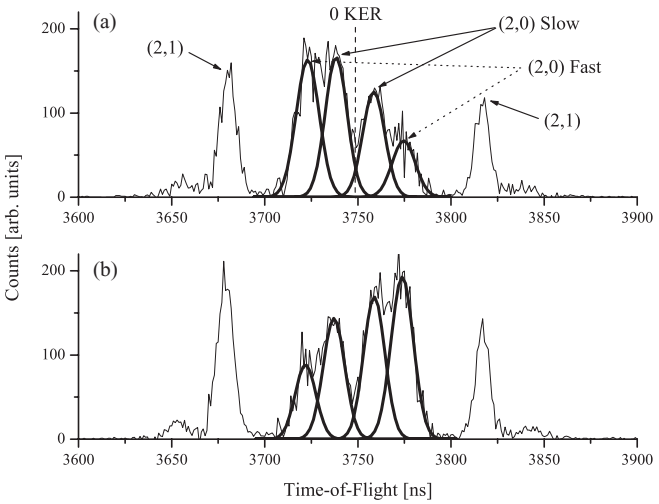

FIG. 8. TOF data showing the two sets of peaks associated with the (2,0) channel at a pump-probe delay of 130 fs ($R = 7.4$ a.u.). The peaks are symmetric about the 0 KER line. The solid lines represent Gaussian fits to each pair of peaks for (a) TOF at $\phi = \pi$ and (b) TOF at $\phi = 0$.

model. However, the left-right asymmetry measurement does not fully take advantage of our TOF resolution: It simply provides a measurement of all the detected ions within a range of KER which are initially toward or away from the detector. In fact, closer examination of the (2,0) TOF measurements reveals that multiple peaks which we attribute to two different (2,0) channels can be resolved (Fig. 8). It is therefore pertinent to examine each of the (2,0) channels and perform calculations which are analogous to those done in the left-right asymmetry scenario.

Fitting each set of (2,0) peaks with Gaussians as shown in Fig. 8 results in two different sets of data: the slow (low energy) and fast (higher energy) channels. The asymmetry of

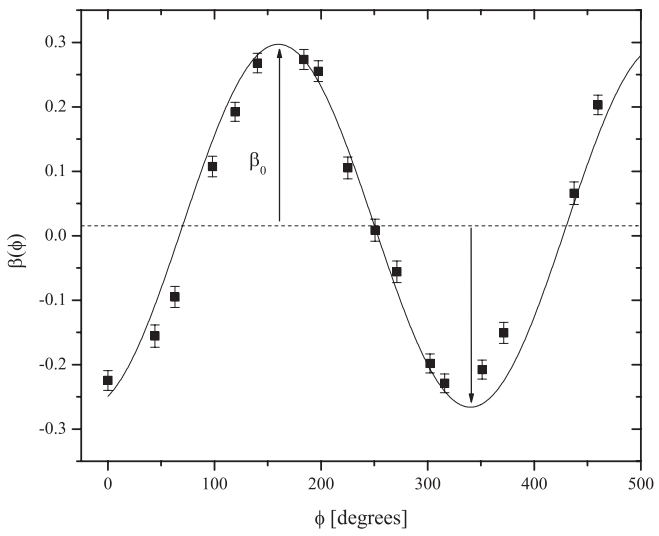

FIG. 9. Example of the left-right asymmetry vs relative phase ϕ for the (2,0) channel at 130 fs pump-probe delay. The solid line is a sinusoidal fit using Eq. (3). The arrows indicate the amplitude of the asymmetry β_0.

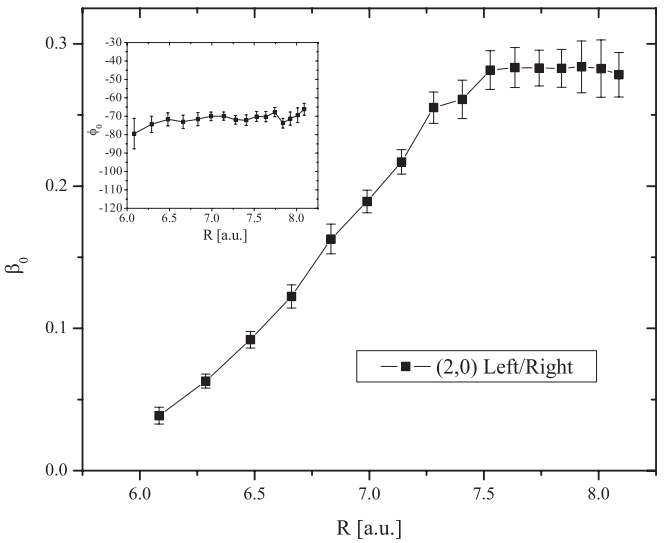

FIG. 10. Measured amplitude of the asymmetry β_0 for the left-right asymmetry of the (2,0) channel. The inset shows the phase ϕ_0 vs R with a vertical scale of 90°.

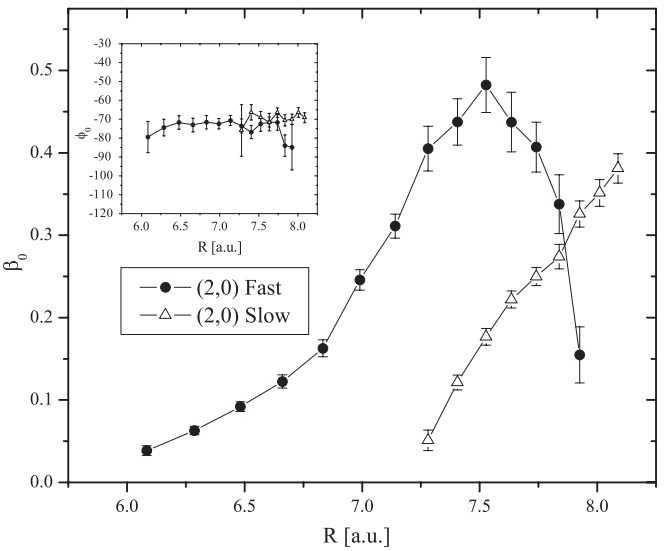

FIG. 12. Measured amplitude of the asymmetry β_0 for each of the observed (2,0) channels. The inset shows the phase ϕ_0 vs R with a vertical scale of 90°.

both the slow and the fast channels show a clear dependence on the $1\omega 2\omega$ phase similar to Fig. 9. The amplitude of the asymmetry β_0 as a function of R for each (2,0) channel is presented in Fig. 12. Here β_0 is also an increasing function of R at small R. The slow channel is just resolved at about 7.25 a.u. and β_0 increases monotonically with R up to about 8 a.u. when the signal from the (2,0) disappears. The fast channel also increases with R up until about 7.5 a.u., when it reaches a maximum. As R increases, β_0 increases from 0 up to about 0.50 for the (2,0) channels, as shown in Fig. 12, while ϕ_0 stays constant within the error bars (see inset).

Although our two-level model predicts a maximum asymmetry of 1, our experimental setup is not optimized for measuring spatial asymmetry due to the difference in angular acceptance for the forward and backward peaks, discussed above. Therefore, the resulting measured asymmetries may be slightly lower than expected. Some groups use velocity map imaging (VMI) to measure ion yields resulting in asymmetry measurements as high as ±0.7 [29]. Nevertheless, both of the (2,0) channels show an increase in the amplitude of the asymmetry as a function of R and a constant ϕ_0. Each channel has a distinct dependence as seen in Fig. 12, again suggesting the presence of two distinct pairs of CR states. Figure 13 shows the results of the β_0 based on the two-level model for two different dipole couplings. The offset in $\beta_0(R)$ as seen in Fig. 12 could be due to the different dipole couplings of the two states.

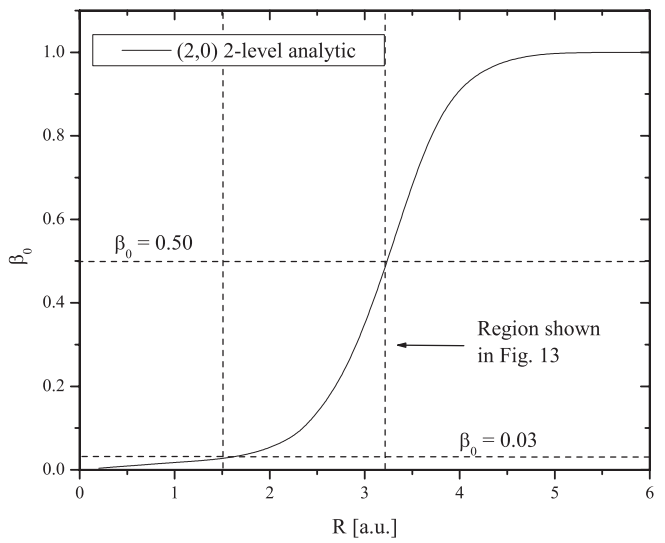

FIG. 11. Analytic calculation of the amplitude of the asymmetry, β_0, for one (2,0) channel. The minimum and maximum asymmetries measured experimentally are indicated by the dashed horizontal lines.

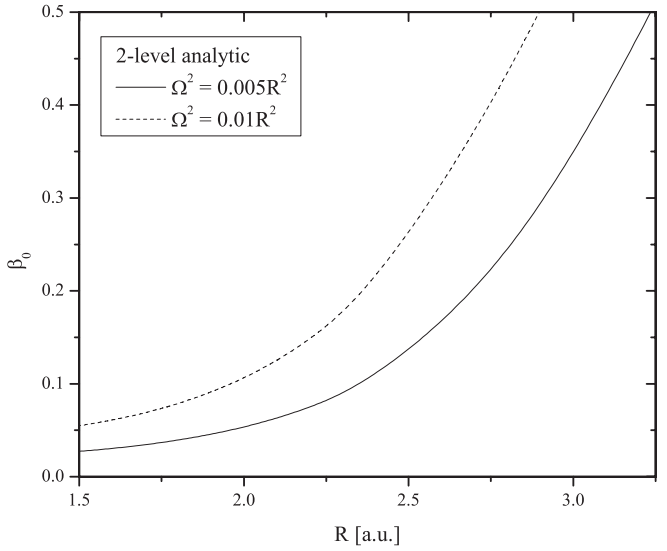

FIG. 13. Analytic calculation of β_0 for two different couplings in the range of values measured experimentally. The asymmetry is monotonically increasing with R in this region. The different couplings of the CR states may be related to the results of Fig. 12.

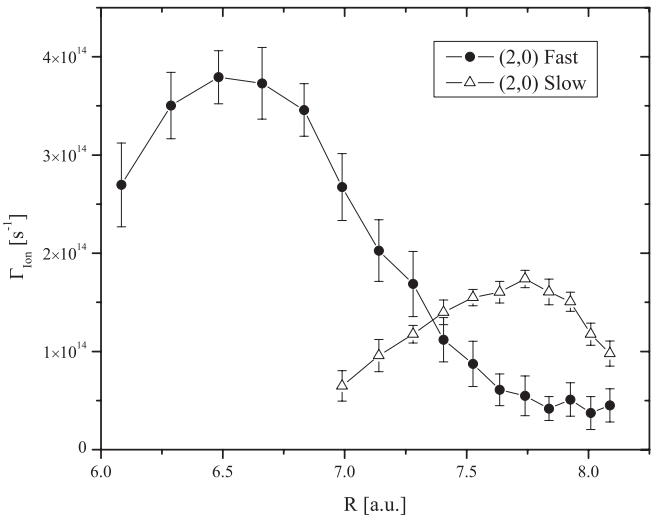

FIG. 14. Ionization rates vs internuclear separation for each of the (2,0) channels. Each (2,0) state has a different critical internuclear separation.

Up to this point, the results are still in qualitative agreement with our two-level model as well as the results of the left-right asymmetry measurements. However, the maximum in the amplitude of the asymmetry is not predicted by the model. The molecule *must* approach the separated atom limit at which point there can be no asymmetry, although nonadiabatic effects and dephasing may play a role as well. The R at which the molecule begins to behave as two separated atoms is not well known and the physics in this region may be important in understanding molecules on a fundamental level. The observation of a maximum in β_0 may indicate this transition region, at which point our two-level model loses validity as it assumes adiabatic following of the field.

The R dependence of the ionization into the (2,0) channels is also measured. Figure 14 shows the ionization rates into the (2,0) channels based on the total counts measured in the TOF. The total counts are found by summing each pair of forward and backward peaks [i.e., the (2,0) slow peaks]. The most prominent features are the two peaks of (2,0) occurring at different R's. The R at which the slow peaks show a maximum is around 6.5 a.u. (70 fs) and the fast peaks show a maximum at around 7.7 a.u. (160 fs). Again, the observation of two peaks in the ionization is evidence for populating two different (2,0) channels [16].

IV. DISCUSSION

The observation of charge asymmetric dissociation (CAD) channels in homonuclear diatomic molecules presents an interesting challenge to understanding the behavior of molecules in strong laser fields. Most work in this field focuses on the ionization rate of the ground state of the molecule as a function of internuclear separation and alignment and one would not necessarily consider the possibility that this would lead to excitation of the resulting molecular ion. Nevertheless, as mentioned in the Introduction, the ionic states leading to CAD are indeed electronically excited and this excitation energy can be quite substantial (up to 8.7 eV in I_2^{2+} and 30 eV in N_2^{6+}). Thus, we would like to get a better understanding of the mechanism behind this extraordinary degree of excitation.

There are two possible routes to populating the states leading to CAD in even-charged molecules: (1) Ionization of the previous charge state directly populates the ionic states, and (2) ionization of the previous charge state leaves the ion in the covalent charge-symmetric ground state and the ion is further excited by the laser field to the high-lying ionic states. Both possibilities have connections to prior theoretical work. Bandrauk *et al*. found that the ionic states play an important role in the ionization of even-charged molecules, but they did not consider ionization *into* the ionic states. It has also been shown that the covalent ground state and gerade-ungerade ionic states form an interesting three-level system that can support very high-order (>10) multiphoton transitions [35]. Indeed, evidence was found for a resonant three-photon transition in I_2^{2+} [36]. Nevertheless, we think that it is unlikely that the (2,0) states are being populated by resonant mulitphoton transitions in this experiment.

This simple observation of spatially asymmetric dissociation means that both the gerade and ungerade states must be coherently populated such that they add or subtract to produce the higher charged ion going either forward or backward with respect to the detector (see the Appendix). Since the singlet covalent ground state has gerade symmetry, a single-color laser field will resonantly couple to only one of the ionic states (gerade or ungerade), depending on the number of photons involved. This is why a single color cannot produce spatial asymmetry. If the second harmonic is added, the selection rules change, raising the possibility that both gerade and ungerade states can be populated, but only under very restrictive conditions: The number of photons absorbed from the 2ω beam must be odd, so that the number of photons from the 1ω beam is even. With our 800-/400-nm $1\omega 2\omega$ beam, this is not possible considering our knowledge of the potential energy curves of the I_2^{2+} molecule, within the range of R that we can probe. Even if an appropriate R existed where both the gerade and ungerade states could be resonantly populated, it would not explain the systematic dependence of the asymmetry on R.

Thus, we return to the first possibility mentioned above. A simple two-electron one-dimensional (1D) model reveals the basic structure of a even-charged molecular ion (Fig. 15 and the Appendix). The (1,1) channel forms the covalent ground state and the (2,0) gerade-ungerade states are the excited CR pair of states. The CR states have two distinctive features. They become completely degenerate at large R and the dipole coupling between them approaches R as R gets large [35]. Thus, if a dc field is applied, the states are barely perturbed at small R and become quite distorted at large R. Moreover, at small R, the states will only be slightly mixed, whereas at large R, they become fully mixed. To include ionization, we make the ansatz that the lower of the two field-induced states will be preferentially populated when this charge state is created through ionization. With this ansatz, we can predict the amplitude of the spatial asymmetry as a function of R as follows (Fig. 11). At small R, there is little mixing of the CR states and only the ungerade will be populated. Since this state has equal probability of having the

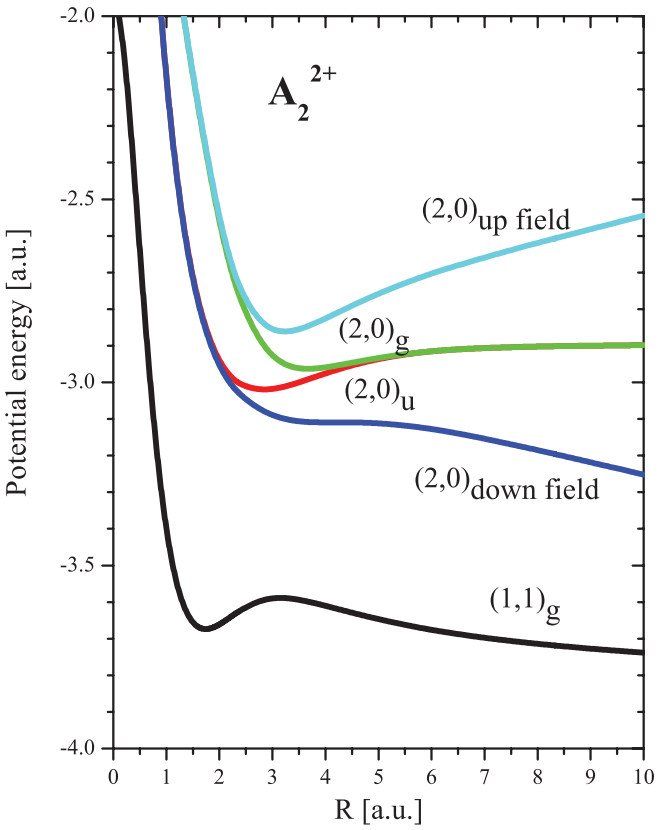

FIG. 15. (Color online) Quasistatic potential energy curves for arbitrary molecular ion A_2^{2+} without field (g and u curves) and with an external static field (up-field and down-field) of 0.07 a.u.

electrons on either ion, there will be no spatial asymmetry. At large R, the states are completely mixed and the lower field-induced state receives all the population. However, this field-induced state is a coherent superposition of the field-free states and this will lead to a maximum spatial asymmetry. Thus, we predict that the spatial asymmetry will start very small at small R and reach a maximum value of 1 at large R. A quantitative calculation of the asymmetry as a function of R is given in the Appendix, within the context of our model. Another consequence of this model is that the phase of the maximum asymmetry will not change as a function of R. This is because the maximum asymmetry will always occur when the field asymmetry is, itself, a maximum. Note, this would not necessarily be true for a resonant multiphoton transition [31].

The above description considered a dc field. In the presence of a single-color ac field, the coherent sum of the field-free states will reverse as the field reverses. In other words, the lower field-induced state will lead to a left-going ion for one direction of the field and a right-going ion for the other direction of the field. In this way, the left- and right-going states will be equally populated leading to no spatial asymmetry. In the two-color field, one direction is preferred over the other, leading to a preference for the left- or right-going ion which will then show a spatial asymmetry.

Our data are consistent with both predictions of the two-level model: The amplitude of the spatial asymmetry β_0 increases with R up to a point and the phase giving rise to the maximum asymmetry ϕ_0 is independent of R. Thus, we conclude that the ionization of I_2^+ can directly populate the excited ionic states of I_2^{2+}. Of course, this implies that if the ionic states are populated, the least bound electron could not have been the one ionized, as, by definition, that would have left the ion in the ground state. This is another example of a phenomena gaining attention lately, namely, excitation through ionization [37]. However, we do not see the asymmetry reach the predicted value of 1 at large R. Instead, we find that β_0 goes through a maximum and then decreases toward zero at large R and our model does not capture this behavior. This is perhaps not so surprising as we have used a dc field and the time-independent Schrödinger equation to study dynamics only as a function of R. A more detailed two-level calculation in which the time dependence of the $1\omega 2\omega$ field is applied may provide insight into the observed maximum and subsequent decrease in β_0 as a function of R.

Finally, we return to our observation of additional structure in the TOF spectrum around the (2,0) channel. From the KER measurements, the ionization rates as a function of R, and the spatial asymmetries, we must conclude that we are populating two distinct (2,0) states, each of which is a CR pair.

V. CONCLUSION

We have measured the spatial asymmetry of the CAD channel of I_2^{2+} as a function of internuclear separation by first exciting the neutral molecule to the B state and letting it evolve in time. By varying the delay of a $1\omega 2\omega$ probe pulse, we measure the asymmetry as a function of internuclear separation for different values of the $1\omega 2\omega$ phase. The maximum amplitude of the spatial asymmetry increases with R, goes through a maximum, and then decreases while the phase of the maximum asymmetry is constant. By comparing these results to a simple two-level model in a dc field, we conclude that the molecules are ionized directly into the field-dressed ionic states of the dication. Although our two-level model captures many of the characteristics of the spatial asymmetry, it appears to break down as it does not predict the behavior of the asymmetry for all observed values of R. In addition, we find evidence for two different states correlating with the $I^{2+} + I$ dissociation limit. Finally, we observe spatial asymmetries for the states with dissociation limits with a charge difference of 2, but not for a charge difference of 1.

ACKNOWLEDGMENT

We would like to acknowledge support from the NSF under Grant No. PHYS-0968799.

APPENDIX: THE MODEL TWO-LEVEL SYSTEM

To model the spatial asymmetry of the (2,0) channel, we use the following Hamiltonian that corresponds to two electrons in a 1D double-well potential and captures the ground and ionic state three-level structure of a dication [35]: $H(t) = H_s(t) + H_p(t)$, where $H_p(p_1,p_2,t) = p_1^2/2 + p_2^2/2$ and

$$H_s(x_1,x_2,t) = \frac{-Z}{\sqrt{(x_1-d)^2+a^2}} + \frac{-Z}{\sqrt{(x_1+d)^2+a^2}}$$

$$+\frac{-Z}{\sqrt{(x_2-d)^2+a^2}}+\frac{-Z}{\sqrt{(x_2+d)^2+a^2}}$$
$$+\frac{1}{\sqrt{(x_1-x_2)^2+a^2}}, \tag{A1}$$

$R = 2d$ is the internuclear separation, a is a smoothing parameter, $Z = 2$ is the charge on each atom, and r_1, r_2 (p_1, p_2) are the positions (momenta) of the electrons. This Hamiltonian produces the field-free potential curves show in Fig. 15.

We then consider just the two-level subsystem, namely, the (2,0) g and u states:

$$H_0(R) = \begin{pmatrix} E_u(R) & 0 \\ 0 & E_g(R) \end{pmatrix}, \tag{A2}$$

where the eigenstates are $(2,0)_g$ and $(2,0)_u$ (Fig. 15) and are defined as $|g\rangle$ and $|u\rangle$ as follows:

$$\begin{aligned} H_0|u\rangle &= E_u|u\rangle, \\ H_0|g\rangle &= E_g|g\rangle, \\ |u\rangle &= \begin{pmatrix} 1 \\ 0 \end{pmatrix}, \\ |g\rangle &= \begin{pmatrix} 0 \\ 1 \end{pmatrix}. \end{aligned} \tag{A3}$$

The strong field couples the two states resulting in the Hamiltonian:

$$H = \begin{pmatrix} E_u & \Omega \\ \Omega & E_g \end{pmatrix}, \tag{A4}$$

where $\Omega \approx \alpha R$ in atomic units and α corresponds to the electric field. For $R > 2$, the dipole matrix element $\langle u|\, r_1 + r_2\, |g\rangle$ is approximately R [35]. In the presence of the electric field, the potential curves will be modified, as shown in Fig. 15 and are defined as the up-field and down-field states. The static field breaks the degeneracy of the g and u levels and the states in Eq. (A3) are no longer eigenstates of the Hamiltonian Eq. (A4). To find the new eigenstates in the field we first find the eigenvalues of Eq. (A4) and define them as

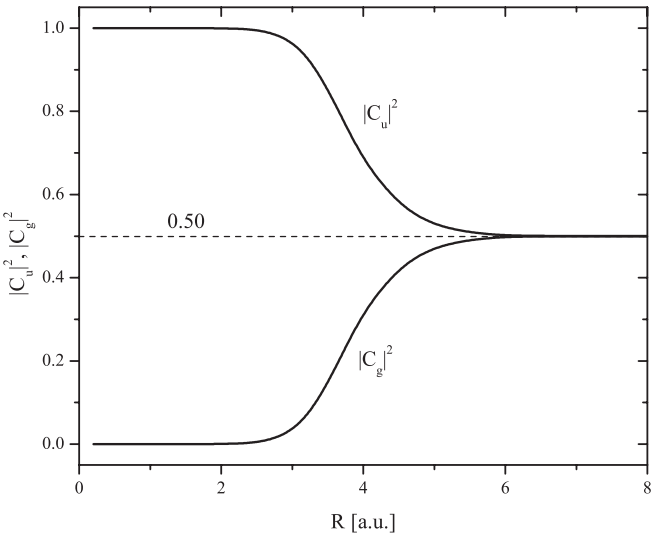

FIG. 16. Probabilities based on the coefficients of the field-induced state $|\psi^-\rangle$ in Eq. (A7). As the states become degenerate, the populations approach 50%.

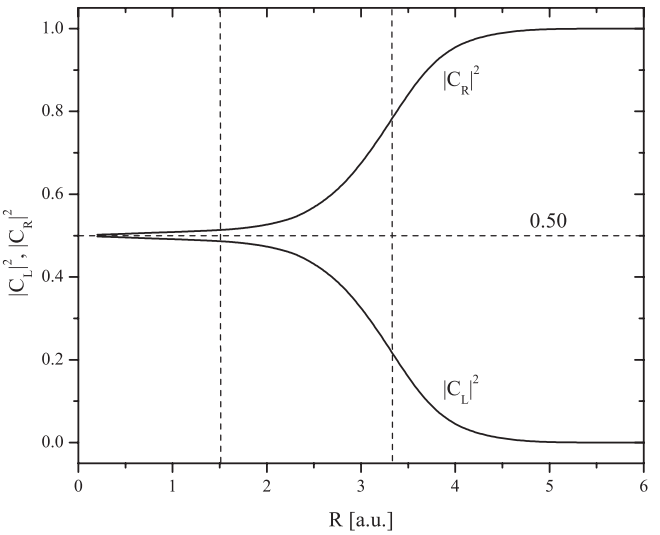

FIG. 17. Probabilities based on the coefficients of Eq. (A13), which are used to calculate β_0. The range for the minimum and maximum asymmetries measured experimentally are indicated by the dashed vertical lines. At small R β_0 is small and as R increases β_0 approaches a maximum of one as shown in Fig. 11.

$$\lambda_\pm = \Sigma \pm \Delta\sqrt{1+\left(\frac{\Omega}{\Delta}\right)^2}, \tag{A5}$$

$$\begin{aligned} \Sigma &\equiv \frac{E_u + E_g}{2}, \\ \Delta &\equiv \frac{E_u - E_g}{2}, \end{aligned} \tag{A6}$$

where λ_+ (λ_-) corresponds to the up-field (down-field) quasistatic energy. We define the eigenstates of Eq. (A4) as $|\psi^+\rangle$ for the up-field state associated with λ_+ and $|\psi^-\rangle$ for the down-field state associated with λ_- in terms of the original basis states in Eq. (A3) as

$$\begin{aligned} |\psi^+\rangle &= C_{g+}|g\rangle + C_{u+}|u\rangle, \\ |\psi^-\rangle &= C_{g-}|g\rangle + C_{u-}|u\rangle \end{aligned} \tag{A7}$$

(see Fig. 16). Equations (A5) and (A7) allow us to solve for the amplitudes under the normalization condition that

$$C_{g\pm}^2 + C_{u\pm}^2 = 1, \tag{A8}$$

where the amplitudes in Eq. (A7) are defined as

$$\begin{aligned} \frac{C_{g+}}{C_{u+}} &= \frac{1+\sqrt{1+\left(\frac{\Omega}{\Delta}\right)^2}}{\left(\frac{\Omega}{\Delta}\right)} \equiv N_+, \\ \frac{C_{g-}}{C_{u-}} &= \frac{1-\sqrt{1+\left(\frac{\Omega}{\Delta}\right)^2}}{\left(\frac{\Omega}{\Delta}\right)} \equiv N_-. \end{aligned} \tag{A9}$$

The amplitudes in Eq. (A7) can then be found from Eqs. (A8) and (A9):

$$C_{g\pm} = \frac{N_\pm}{\sqrt{1+N_\pm^2}}, \qquad C_{u\pm} = \frac{1}{\sqrt{1+N_\pm^2}}. \tag{A10}$$

The eigenstates of Eq. (A4) in terms of the field-free $|g\rangle$ and $|u\rangle$ basis are therefore

$$|\psi^+\rangle = \frac{N_+}{\sqrt{1+N_+^2}}|g\rangle + \frac{1}{\sqrt{1+N_+^2}}|u\rangle, \qquad |\psi^-\rangle = \frac{N_-}{\sqrt{1+N_-^2}}|g\rangle + \frac{1}{\sqrt{1+N_-^2}}|u\rangle. \tag{A11}$$

At this point we have a full description of the the two-level system in the laser field. We propose that there will be preferential ionization to the down-field state $|\psi^-\rangle$ since it lies at a lower energy than the up-field state of the system. Since $|\psi^-\rangle$ contains both $|u\rangle$ and $|g\rangle$ components, population of this state can lead to spatially asymmetric dissociation. In the laser field, the eigenstates are a coherent superposition of the field-free states according to

$$|L\rangle = \frac{|g\rangle + |u\rangle}{\sqrt{2}}, \qquad |R\rangle = \frac{|g\rangle - |u\rangle}{\sqrt{2}}, \tag{A12}$$

where $|L\rangle$ and $|R\rangle$ are left and right going states.

The sudden projection of the down-field $|\psi^-\rangle$ onto this basis gives us the amplitudes of the electronic wave functions going to the left and right:

$$\langle L|\psi^-\rangle = \frac{C_{g-} + C_{u-}}{\sqrt{2}} \equiv C_L, \qquad \langle R|\psi^-\rangle = \frac{C_{g-} - C_{u-}}{\sqrt{2}} \equiv C_R, \tag{A13}$$

where C_L is the amplitude of the wave function in the left well and C_R is the amplitude of the wave function in the right well. Finally, we can calculate the spatial asymmetry based on the two-level system by squaring the amplitudes found in Eq. (A13) and using Eq. (2). The populations in the left and right wells are shown in Fig. 17. The amplitude of the asymmetry β_0 using the results of Eq. (A13) is shown in Fig. 11.

[1] P. Dietrich, M. Yu. Ivanov, F. A. Ilkov, and P. B. Corkum, Phys. Rev. Lett. **77**, 4150 (1996).
[2] M. Ivanov, T. Seideman, P. Corkum, F. Ilkov, and P. Dietrich, Phys. Rev. A **54**, 1541 (1996).
[3] L. J. Frasinski, C. R. Courtney, and K. Codling, J. Mod. Optics **50**, 485 (2003).
[4] C. Cornaggia, J. Lavancier, D. Normand, J. Morellec, and H. X. Liu, Phys. Rev. A **42**, 5464 (1990).
[5] C. Guo, M. Li, and G. N. Gibson, Phys. Rev. Lett. **82**, 2492 (1999).
[6] G. N. Gibson, M. Li, C. Guo, and J. P. Nibarger, Phys. Rev. A **58**, 4723 (1998).
[7] J. P. Nibarger, S. V. Menon, and G. N. Gibson, Phys. Rev. A **63**, 053406 (2001).
[8] J. P. Nibarger, M. Li, S. Menon, and G. N. Gibson, Phys. Rev. Lett. **83**, 4975 (1999).
[9] L. J. Frasinski, K. Codling, P. Hatherly, J. Barr, I. N. Ross, and W. T. Toner, Phys. Rev. Lett. **58**, 2424 (1987).
[10] P. Dietrich, D. T. Strickland, M. Laberge, and P. B. Corkum, Phys. Rev. A **47**, 2305 (1993).
[11] L. Quaglia and C. Cornaggia, Phys. Rev. Lett. **84**, 4565 (2000).
[12] T. Zuo and A. D. Bandrauk, Phys. Rev. A **52**, 2511 (1995).
[13] E. Constant, H. Stapelfeldt, and P. B. Corkum, Phys. Rev. Lett. **76**, 4140 (1996).
[14] R. Bavli and H. Metiu, Phys. Rev. Lett. **69**, 1986 (1992).
[15] T. Seideman, M. Yu. Ivanov, and P. B. Corkum, Phys. Rev. Lett. **75**, 2819 (1995).
[16] A. Saenz, Phys. Rev. A **61**, 051402 (2000).
[17] K. Codling, L. J. Frasinski, and P. A. Hatherly, J. Phys. B **22**, L321 (1989).
[18] I. Kawata, H. Kono, Y. Fujimura, and A. D. Bandrauk, Phys. Rev. A **62**, 031401 (2000).
[19] P. H. Bucksbaum, A. Zavriyev, H. G. Muller, and D. W. Schumacher, Phys. Rev. Lett. **64**, 1883 (1990).
[20] R. N. Coffee, L. Fang, and G. N. Gibson, Phys. Rev. A **73**, 043417 (2006).
[21] R. S. Mulliken, J. Chem. Phys. **7**, 20 (1939).
[22] H. Yu, T. Zuo, and A. D. Bandrauk, Phys. Rev. A **54**, 3290 (1996).
[23] R. N. Coffee and G. N. Gibson, Phys. Rev. A **72**, 011401(R) (2005).
[24] T. Zuo, S. Chelkowski, and A. D. Bandrauk, Phys. Rev. A **48**, 3837 (1993).
[25] I. Kawata, H. Kono, Y. Fujimura, and A. D. Bandrauk, Phys. Rev. A **62**, 031401(R) (2000).
[26] K. Harumiya, H. Kono, Y. Fujimura, I. Kawata, and A. D. Bandrauk, Phys. Rev. A **66**, 043403 (2002).
[27] A. D. Bandrauk and S. Chelkowski, Phys. Rev. Lett. **84**, 3562 (2000).
[28] B. Sheehy, B. Walker, and L. F. DiMauro, Phys. Rev. Lett. **74**, 4799 (1995).
[29] K. J. Betsch, D. W. Pinkham, and R. R. Jones, Phys. Rev. Lett. **105**, 223002 (2010).
[30] S. De *et al.*, Phys. Rev. Lett. **103**, 153002 (2009).
[31] D. Ray *et al.*, Phys. Rev. Lett. **103**, 223201 (2009).
[32] L. Fang and G. N. Gibson, Phys. Rev. A **81**, 033410 (2010).
[33] C. Guo, M. Li, J. P. Nibarger, and G. N. Gibson, Phys. Rev. A **58**, R4271 (1998).
[34] W. C. Wiley and I. H. McLaren, Rev. Sci. Instrum. **26**, 1150 (1955).
[35] G. N. Gibson, Phys. Rev. A **67**, 043401 (2003).
[36] G. N. Gibson, R. N. Coffee, and L. Fang, Phys. Rev. A **73**, 023418 (2006).
[37] L. Fang and G. N. Gibson, Phys. Rev. Lett. **100**, 103003 (2008).
[38] L. Fang and G. N. Gibson, Phys. Rev. A **75**, 063410 (2007).